Targeting SARS-CoV-2 main protease by teicoplanin: a mechanistic insight by *in silico* studies

Faizul Azam*

Department of Pharmaceutical Chemistry & Pharmacognosy, Unaizah College of Pharmacy, Qassim University, Unaizah, Saudi Arabia

*Corresponding author Tel +966-50-2728652; E-mail: faizulazam@gmail.com; f.azam@qu.edu.sa

Graphical Abstract

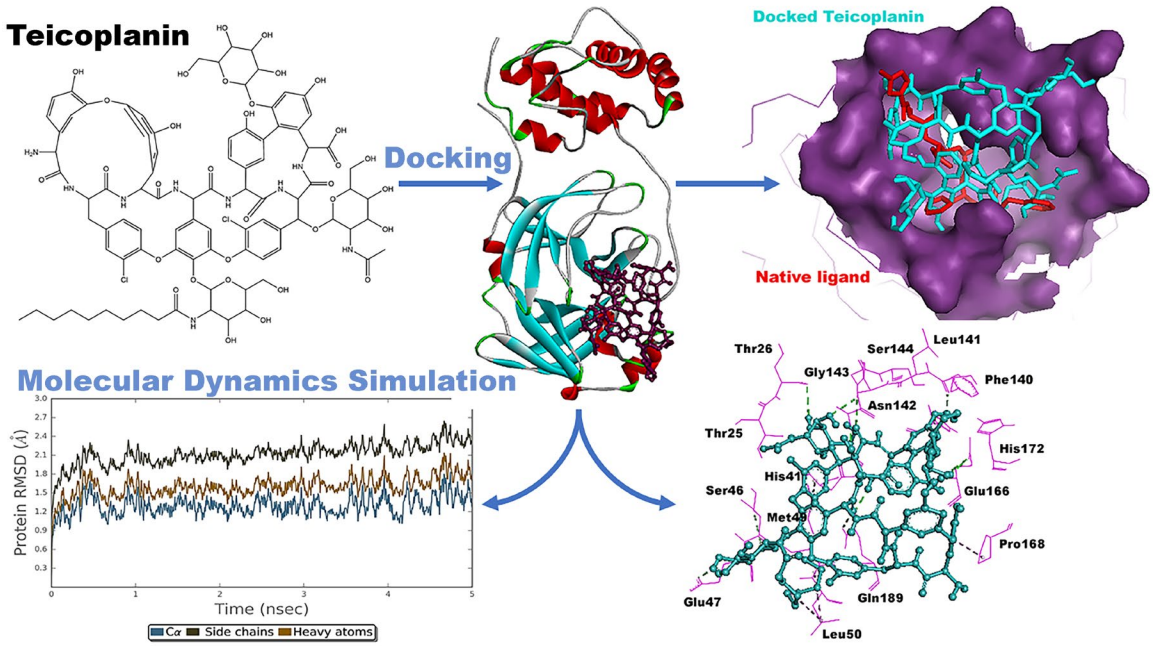

Abstract

First emerged in late December 2019, the outbreak of novel severe acute respiratory syndrome corona virus-2 (SARS-CoV-2) pandemic has instigated public-health emergency around the globe. Although available medications can only alleviate few symptoms like difficulty in breathing, the world is craving to identify specific antiviral agents or vaccines against SARS-CoV-2. Teicoplanin is a glycopeptide class of antibiotic which is regularly used for treating Gram-positive bacterial infections, has shown potential therapeutic efficacy against SARS-CoV-2 *in vitro*. Therefore, in this study, a mechanistic insight of intermolecular interactions between teicoplanin and SARS-CoV-2 main protease has been scrutinized by employing molecular modelling approaches. Molecular docking study was carried out by three different docking programs including AutoDock4, AutoDock Vina and Dock6. The dynamic and thermodynamics constraints of docked drug in complex with target protein under specific physiological conditions was ascertained by all-atom molecular dynamics (MD) simulation study. Root mean square deviation of carbon α chain exhibited uniform value in the range of 1-1.7 Å while root mean square fluctuations were also recorded below 1.72 Å, justifying the stability of the bound complex in biological environments. Key interacting residues involved in hydrogen bonds include Thr26, His41, Asn142, Ser144, Glu166, and Gln189. Several water bridges and hydrophobic interactions also anchored docked teicoplanin in the inhibitor binding site. These outcomes are supposed to be fruitful in rational design of antiviral drugs against SARS-CoV-2.

Keywords: Coronavirus; SARS-CoV-2 protease; teicoplanin; docking; molecular dynamics

1. Introduction

The World Health Organization has declared the ongoing outbreak of coronavirus as a global public-health emergency. First emerged in late December 2019, the novel severe acute respiratory syndrome corona virus-2 (SARS-CoV-2) pandemic has instigated an alarming situation around the globe (Huang et al 2020). Within 4-5 months of its inception, it has invaded 210 countries and territories around the world, reaching 2,714,366 cases till date, April 24, 2020 and the count is still increasing every day. Till date, there is no specific therapeutic regimen for the treatment of this devastating SARS-CoV-2 viral infection. Although available medications can only alleviate few symptoms like difficulty in breathing, the world is craving to identify specific antiviral agents or vaccines against SARS-CoV-2 (Raoult et al 2020).

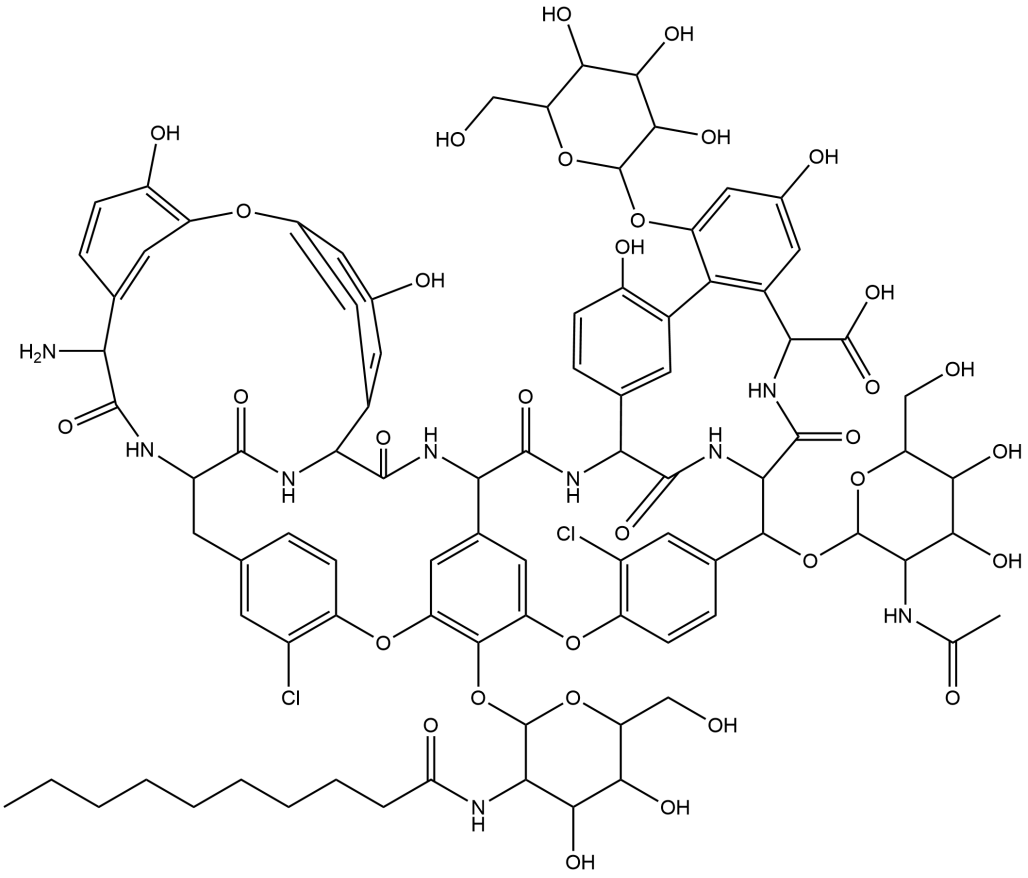

Fig. 1. Chemical structures of the teicoplanin used in present study.

Teicoplanin (Figure 1) is widely available, FDA-approved glycopeptide type of antibiotic with low toxicity profile in humans. It is routinely used in clinical practice for the treatment of bacterial infections. However, it has shown anti-viral activity against SARS-CoV, MERS-CoV and Ebola virus *in vitro* via specifically inactivating the activity of cathepsin L, a cysteine peptidase enzyme (Zhou et al., 2016). Very recently, same research group has disclosed that teicoplanin can prevent the cellular entry of SARS-CoV-2 at 1.66 μM concentration (Zhang et al, 2020).

Computer-aided drug design techniques are routinely employed in drug design and discovery projects owing to several advantages such as rapid development process and reduced cost (Aanouz et al, 2020; Azam et al., 2018; Ahmed et al., 2012). In particular, molecular docking coupled with molecular dynamics simulation studies are intended to decipher the mechanism of binding interactions at the molecular levels. Rapid mechanistic insight is vital for understanding structure-activity relationship and lead optimization for the design and discovery of potential molecules (Shushni et al., 2013; Azam et al., 2012). In this study, molecular docking and molecular dynamics protocols were exploited to inspect the binding interactions between teicoplanin and recently solved X-ray crystal structure of SARS-CoV-2 main protease. The study is envisioned to assist in finding potential leads and accelerate drug development process for the treatment of novel coronavirus, COVID-19.

2. Materials and Methods

2.1. Computational details

All the computational calculations were performed on CentOS 7 Linux platform running on hp Workstation with Intel® Core™ i9-9900K CPU @ 3.6 GHz processor and 8 GB of RAM.

2.2. Protein and ligand preparation

Three-dimensional X-ray crystal structure of COVID-19 main protease in complex with an inhibitor N-[(5-methylisoxazol-3-yl)carbonyl]alanyl-L-valyl-N~1~-((1R,2Z)-4-(benzyloxy)-4-oxo-1-{[(3R)-2-oxopyrrolidin-3-yl]methyl}but-2-enyl)-l-leucinamide (N3; PDB ID: 6LU7) was retrieved from Protein Data Bank (Jin et al., 2020). Initial processing of the protein structure was performed in Biovia Discovery Studio 2020 and PyMOL 1.7.4 for removing the solvent and the co-crystallized molecules. Two-dimensional structure of the teicoplanin was obtained from PubChem database in sdf format and converted to its three-dimensional coordinate by using Open Babel (O'Boyle et al., 2011) program. All non-polar hydrogens were merged, rotatable bonds and torsion tree were defined and prepare_ligand4.py module was used to generate pdbqt file with Gasteiger charges added in MGL Tools 1.5.6. The pdbqt file served as input file for AutoDock 4.2 and AutoDock Vina. However, for Dock 6.9, the ligand was protonated and assigned AM1-BCC charges within Chimera 1.14, and finally saved in mol2 format as input file for next step.

2.3. Molecular docking simulation

2.3.1. AutoDock 4.2

AutoGrid 4.2 was employed to calculate a grid of 60, 60, and 60 points in x, y, and z directions with a grid spacing of 0.375 Å. A distance-dependent function for dielectric

constant was applied for the computation of energetic maps. Applying the active site information pertaining to the native co-crystallized ligand, N3, a grid box center for docking was defined as -9.732, 11.403 and 68.925 in x, y and z directions respectively. AutoDock 4.2 was used for docking simulation involving 100 independent runs by Lamarckian genetic algorithm methodology, adjusting default settings for all other parameters (Morris et al, 1998). At the end of docking, the best pose was analyzed for intermolecular interactions and root mean square deviation (RMSD) calculations using Biovia Discovery Studio Visualizer 2020, LigPlot^{+} 2.2 and PyMol 1.7.4 programs (Fahmy et al., 2020).

2.3.2. AutoDock Vina

The grid box with a spacing of 1 Å and a size of 22 × 24 × 28 pointing in x = − 9.732, y = 11.403 and, z = 68.925 directions was built around the center of the binding site defined by the native co-crystallized ligand, N3. Other parameters of docking were set to default while exhaustiveness value was adjusted to 40.

2.3.3. Dock 6.9

DMS module of Dock 6.9 was used to compute the solvent-accessible molecular surface of the target binding site by adjusting the probe radius of 1.4 Å (Allen et al., 2017). SPHGEN program was employed for the generation of receptor spheres. Spheres covering the binding pocket were selected within 9 Å from the positions of the heavy atoms of the native co-crystallized ligand, N3. The grid box center enclosing the selected spheres was generated with dimension of -12.626, 14.596 and 69.128 Å in x, y and z directions respectively. Ligand flexibility was adopted in docking while keeping the protein structure as rigid moiety.

2.4. Molecular dynamics simulation

The best ranked conformation of teicoplanin furnished by docking experiments in complex with SARS-CoV-2 main protease was further examined for assessing their thermodynamic behavior and stability by using MD simulation studies employing Desmond 5.9 academic version (Desmond Molecular Dynamics System 2018; Bowers et al., 2006). System setup protocol was used for placing the ligand-protein complex into an orthorhombic box filled with 10258 water molecules. Simple point charge (SPC) model and OPLS3 force field was adopted for the MD computations (Harder et al., 2016). The system was neutralized using appropriate numbers of (31 Na^+ and 29 Cl^-) counter ions with fixed salt concentration of 0.15M that represents the physiological concentration of monovalent ions. Isothermal-isobaric (NPT) ensemble was employed with temperature and pressure adjusted to 300 K and 1.01325 bar, respectively. A simulation time of 5 ns was adjusted whereas trajectories were saved at every 5 ps. A cut-off radius of 9.0 Å was used for short-range van der Waals and Coulomb interactions. Nose–Hoover thermostat (Hoover, 1985) and Martyna–Tobias–Klein (Martyna, Tobias, & Klein, 1994) methods were employed for maintaining the system temperature and pressure, respectively. In order to integrate the equations of motion, RESPA integrator was used with an inner time step of 2.0 fs for bonded as well as non-bonded interactions within the short-range cut-off (Humphreys et al., 1994). The system was minimized and equilibrated with the default protocols of the Desmond. Simulation event analysis, simulation quality analysis and simulation interaction diagram protocols of the Desmond package was exercised to analyze the trajectory files.

3. Results and Discussion

3.1. Validation of docking protocol

Validation of the implemented docking protocols in AutoDock 4.2, AutoDock Vina and Dock 6.9 was performed by re-docking of native co-crystallized ligand, N3 in the binding pocket of SARS-CoV-2 main protease. The RMSD of the best docked conformation of N3 and X-ray crystal structure were within 2Å for all of the three docking programs used in this study, confirming the reliability of the implemented scoring functions (data not shown). According to the reported protocols, it is evident that for successful docking the RMSD should fall within ≤2.0 Å (Azam et al, 2019, Hussain et al, 2016). Therefore, adopted methodology of the molecular docking used in current study, can be relied to predict the molecular interaction of teicoplanin in the inhibitor binding cavity of SARS-CoV-2 main protease.

3.2. Molecular docking of teicoplanin with SARS-CoV-2 main protease

Molecular docking is a computer-based process of facilitating the early stages of drug discovery through unveiling the mode of binding interactions of chemical compounds as well as systematic pre-screening on the basis of their shape and energetic compatibility with the target proteins (Azam et al, 2015, Ahmed et al, 2016). After successful completion of the docking calculations, best pose with minimum energy conformation of teicoplanin obtained from each docking run was visualized in Biovia Discovery Studio 2020, LigPlot^{+} 2.2 and PyMol 1.7.4 programs to study ligand–protein interactions. As demonstrated in Table 1, docked teicoplanin had ample opportunity within the binding pocket of SARS-CoV-2 main protease to interact by means of both hydrophobic as well as hydrophilic interactions.

Table 1

Results obtained after docking of teicoplanin with SARS-CoV-2 main protease (PDB ID: 6LU7).

Docking program	ΔGb[a] (kcal/mol)	RMSD[c] (Å)	H-Bonds		Hydrophobic interactions		
			Amino acid	Distance (Å)	Type	Amino acid	Distance (Å)
AutoDock 4.2	-1.94	4.73	Thr26	2.84	Alkyl	Met49	5.07
			Ser46	3.37	Alkyl	Leu50	4.31
			Glu47	2.03	π-Alkyl	Leu50	5.42
			Phe140	2.20	π-Alkyl	Pro168	4.31
			Asn142	1.82			
			Gly143	2.89			
			Gly143	2.67			
			His163	2.44			
			Glu166	2.05			
			Glu166	2.66			
			Gln189	2.14			
			Gln189	2.65			
AutoDock Vina	-5.0	4.84	Glu47	2.04	π-Alkyl	Met49	5.17
			Leu141	1.76	Amide- π stacked	Leu167	4.35
			Asn142	2.67	π-Alkyl	Pro168	3.36
			His163	2.78			

			Glu166	2.92			
			Glu166	2.12			
			Glu166	2.55			
			Gln189	1.87			
Dock 6.9	-68.36[b]	5.66	Ser46	3.29	π-Alkyl	Met49	5.05
			Glu47	2.78	π-Alkyl	Pro168	3.83
			Glu47	2.98			
			Leu141	2.34			
			Glu166	2.98			
			Glu166	2.21			
			Glu166	2.29			
			Gln189	2.00			
			Gln189	1.93			

[a] Gibbs free energy of binding (kcal/mol), [b] Grid score, [c] Root mean square deviation.

Results obtained after docking of teicoplanin with SARS-CoV-2 main protease using numerous docking programs clearly revealed that docked teicoplanin accomodated well within inhibitor binding cavity in a similar manner to that of native co-crystallized compound, N3 which is a potent and irreversible inhibitor of COVID-19 virus (Figure 2). Docking poses were compared with N3 by analyzing the root mean square deviation (RMSD). AutoDock 4.2, Autodock Vina 1.1 and Dock 6.9 demonstrated RMSD of 4.73, 4.84 and 5.66 Å, respectively, justifying the AutoDock 4.2 results as most promising.

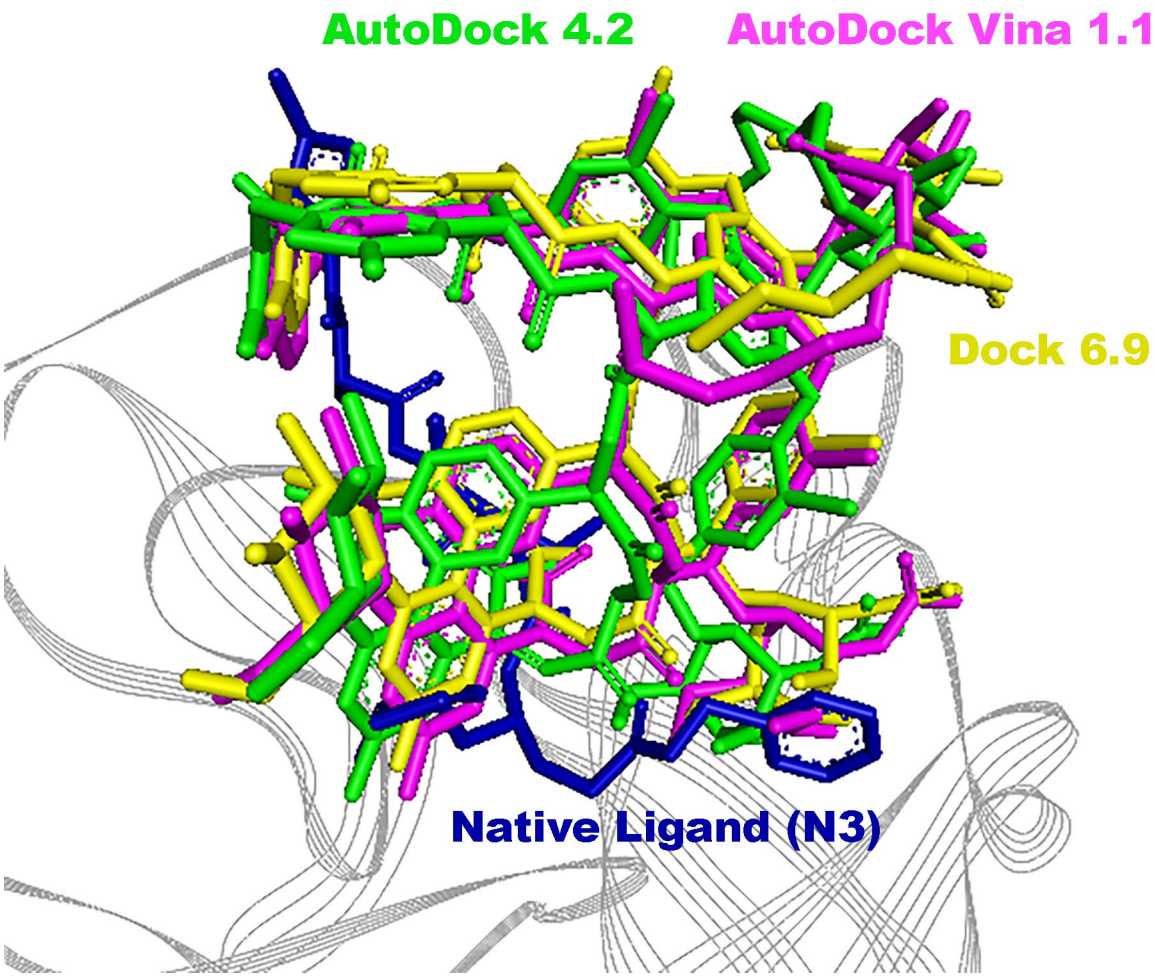

Fig.2. Superimposition of the best docked poses of the teicoplanin on the native co-crystallized ligand pose in the binding pocket of 6LU7. The AutoDock 4.2 pose (in green color), AutoDock Vina 1.1 pose (in magenta color) and the Dock 6.9 pose (in yellow color) has the positional RMSD of 4.73, 4.84 and 5.66 Å, respectively.

X-ray crystal structure of SARS-CoV-2 main protease constitutes three domains comprising 306 amino acid residues (Jin et al., 2020; Enmozhi et al, 2020). Docking poses of teicoplanin furnished by all programs used in current study utilizes mainly domains I and II consisting of residues 8–101 and 102–184, respectively for interaction with the target protein (Figure 3, 4 and 5). Residues of domains I and II form beta-barrels while domain III residues mainly outline alpha-helices. Residues His41 and Cys145 form the catalytic dyad, forming substrate

binding region and located at the cleft of domain I and II in which His acts as a proton acceptor while Cys behaves as a nucleophile. Additional structural features include two deeply buried subsites identified as S1 and S2 whereas three shallow subsites are known as S3-S5. The S1 subsite is composed of Phe140, Gly143, Cys145, His163, Glu166 and His172, but S2 contains Thr25, His41 and Cys145 amino acid residues. S3-S5, known as shallow subsites are capable of tolerating different functionalities and are composed of His41, Met49, Met165, Glu166 and Gln189 amino acid residues (Lu et al. 2006; Jin et al., 2020; Yang et al. 2005).

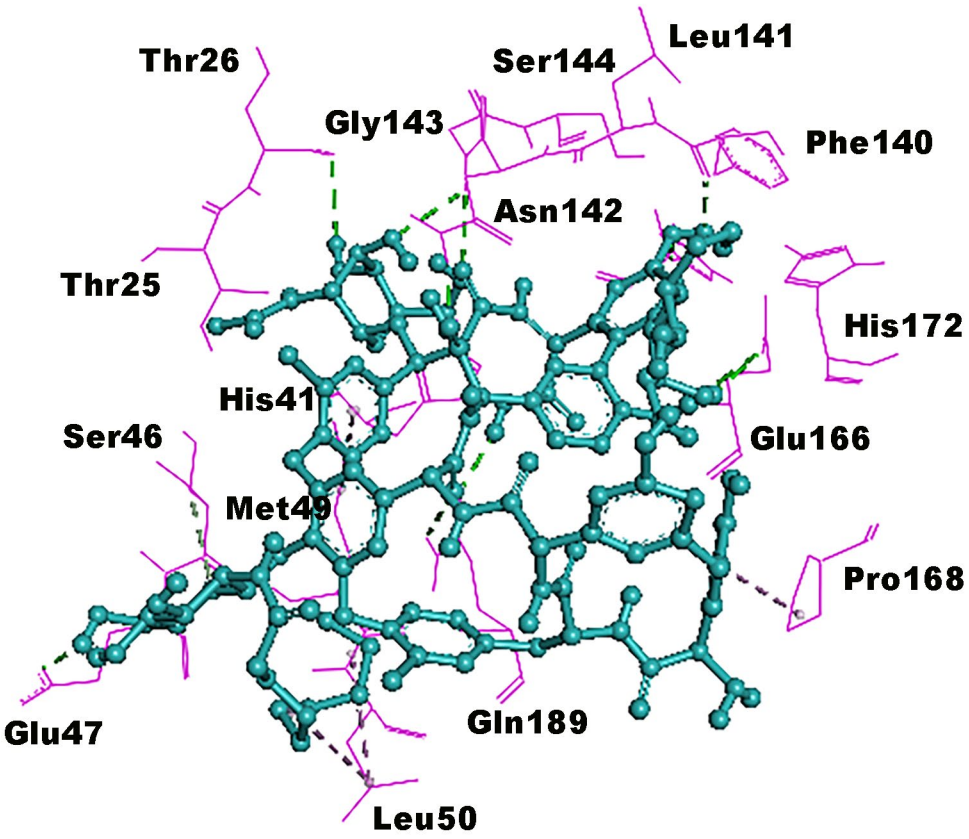

Fig. 3. Best docked pose of teicoplanin (shown as ball and stick in cyan color) by AutoDock 4.2. Residues of the binding pocket are rendered as lines in purple color. Green dotted lines signify hydrogen bonds while hydrophobic interactions are expressed as purple dotted lines.

A combination of numerous H-bond donors/acceptors as well as hydrophobic sites compelled the teicoplanin molecule to interact voraciously within the inhibitor binding pocket of SARS-CoV-2 main protease. AutoDock 4.2 results presented in Figure 3 clearly depicts that Phe140, Gly143, His163 and Glu166 confer H-bond interactions with teicoplanin at the S1 subsite. In addition, Gln189 residue also contributes hydrogen bond interaction, supporting the docked teicoplanin in the shallow subsite (S3-S5) of the binding cavity. However, Leu50 and Pro168 participated in hydrophobic contacts in the form of π-alkyl bonds. Docked conformations of AutoDock Vina 1.1 (Figure 4) and Dock 6.9 (Figure 5) were also involved in hydrophilic contact through Glu166 and Gln189, maintaining the teicoplanin molecule in the S1 subsite. Furthermore, hydrophobic links were noted with Met49 and Pro168 residues.

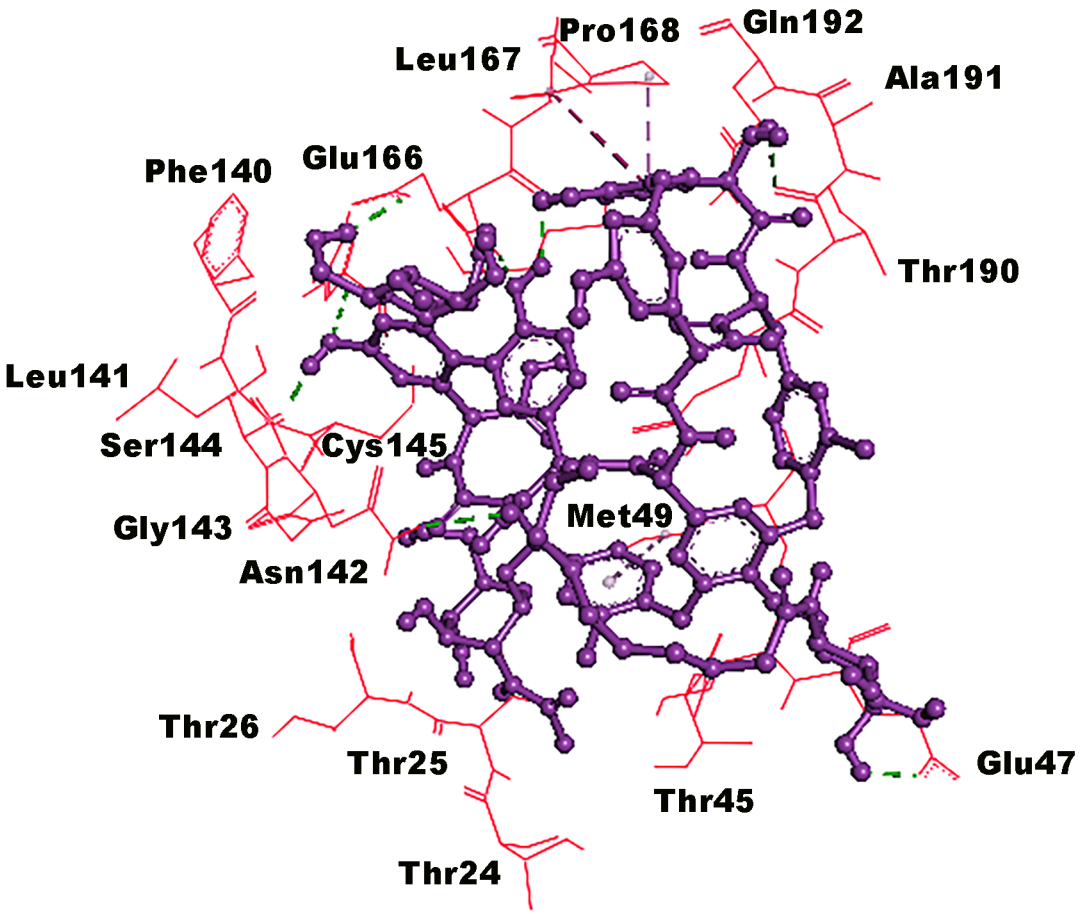

Fig. 4. Best docked pose of teicoplanin (shown as ball and stick in purple color) by AutoDock Vina 1.1. Residues of the binding pocket are depicted as lines in red color.

Hydrogen bonds are designated as green dotted lines whereas hydrophobic interactions are shown as purple dotted lines.

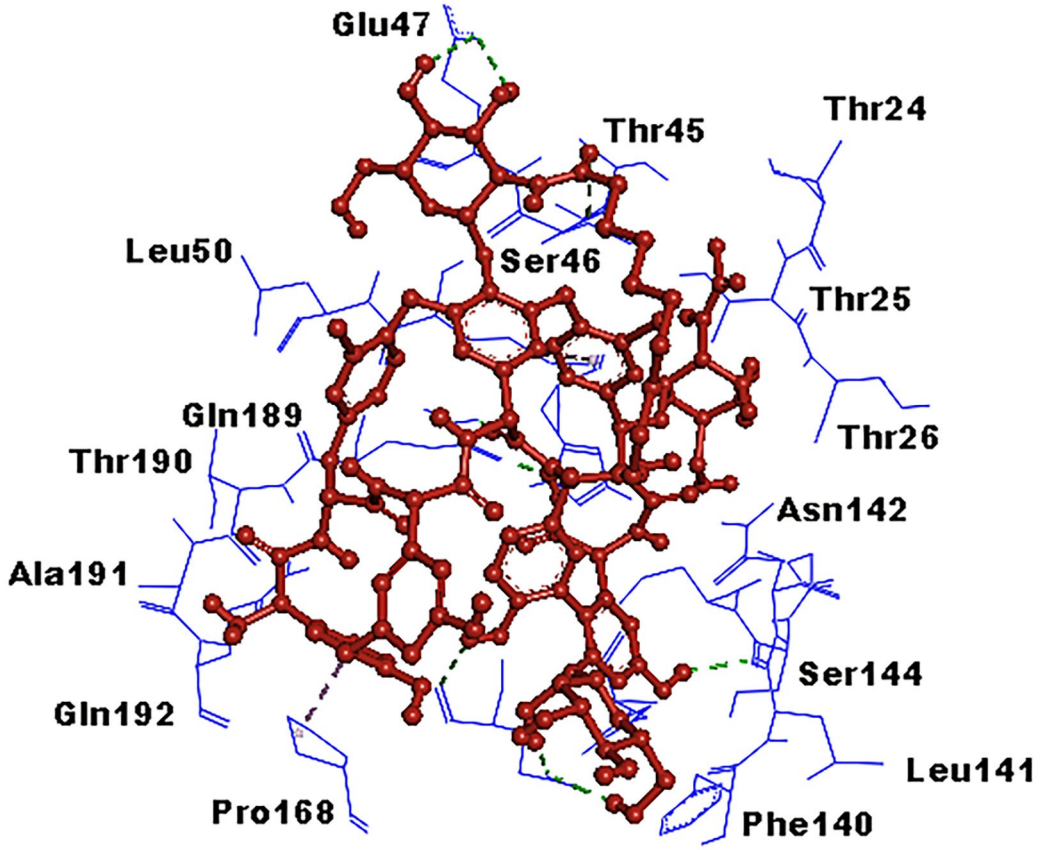

Fig. 5. Best docked pose of teicoplanin (shown as ball and stick in red color) by Dock 6.9. Amino acid residues of the binding pocket are portrayed as lines in blue color. Green dotted lines represent hydrogen bonds and hydrophobic interactions are shown as purple dotted lines.

3.3. Molecular dynamics simulation studies

Dynamic and thermodynamics parameters of living systems under specific conditions of physiological environments can be estimated by the application of molecular dynamics (MD) simulation, a widely employed computer-aided drug design technique (Azam 2018, 2019,

Hospital et al., 2015; Elfiky 2020). Therefore, the best docked pose of teicoplanin in complex with SARS-CoV-2 main protease was subjected to MD simulation study in order to investigate the stability of the ligand-protein complex as well as main intermolecular interactions during the simulated trajectory. Docking pose afforded by AutoDock 4.2 was selected for MD simulation study owing to the minimum RMSD observed between docked teicoplanin pose and native co-crystallized SARS-CoV-2 main protease inhibitor, N3. In addition, superior intermolecular interactions were observed in comparison with AutoDock Vina 1.1 and Dock 6.9 poses. Desmond software was employed for the MD simulation of 5 ns in explicit solvent system. The resulting trajectories of the simulated complex was inspected for different standard simulation parameters such as backbone RMSDs for alpha-carbons, side chains and heavy atoms. In addition, the root mean square fluctuations (RMSFs) of individual amino acid residues, intermolecular interactions involved, and radius of gyration (rGyr) were also evaluated. The RMSD plot of simulated complex is presented in Figure 6. The analysis of RMSD indicates that the simulated system has equilibrated very well because the fluctuations in the Cα atoms were consistently below 1.78 Å during the entire simulated path. However, slight fluctuation can be expected during initial period which acquires stability throughout rest of simulation route. A system showing fluctuation of 1-3 Å is usually considered stable and deemed to be properly equilibrated in case of globular proteins whereas elevated RMSD values are regarded as an indication of large conformational changes in protein structure over the progression of simulation (Wahedi et al, 2020).

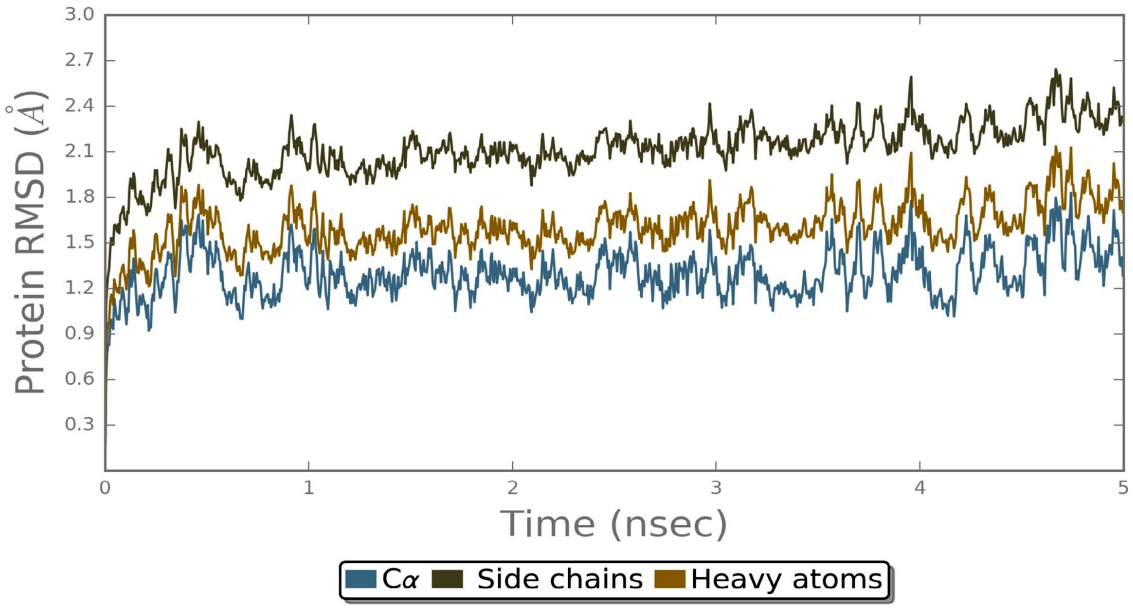

Fig. 6. The Root Mean Square Deviations (RMSD) of Cα, side chains and heavy atoms relative to the starting complex during 5 ns MD simulation of teicoplanin.

The local conformational alterations along SARS-CoV-2 main protease chain were investigated by analyzing the RMSF during simulation time. Loop regions in the RMSF plot has been shown by white bar whereas alpha-helices and beta-sheets are represented in the form of blue and pink bars, respectively. As depicted in Figure 7, loop regions usually fluctuate the most during simulation, though alpha-helices and beta-sheets were rigid. The vertical green lines on the X-axis of the plot illustrate the participation of interacting residues between SARS-CoV-2 main protease chain and teicoplanin. Key residues of H-bond interactions such as Thr26, His41, Ser46, Asn142, Glu166 and Gln189 had maximum RMSFs of 0.56, 0.46, 0.96, 0.83, 0.64 and 0.73 Å, respectively. Important residues sharing hydrophobic interactions such as Met49, Leu50, Met165 and Ala191 displayed RMSFs of 0.68, 0.76, 0.58 and 0.81 Å, respectively. All of these figures were estimated around the flexible loop regions of target protein. As shown in Figure 7, the maximum RMSF corresponding to the terminal residues was reflected by Ser1 and Gln306 as 3.64 and 4.10 Å,

respectively. These residues are located far away from the ligand binding site, and hence, deemed insignificant. Furthermore, the RMSF of the SARS-CoV-2 main protease chain was also correlated with the experimental x-ray B-factor values (shown on the right Y-axis), which is in accordance with the crystallographic data.

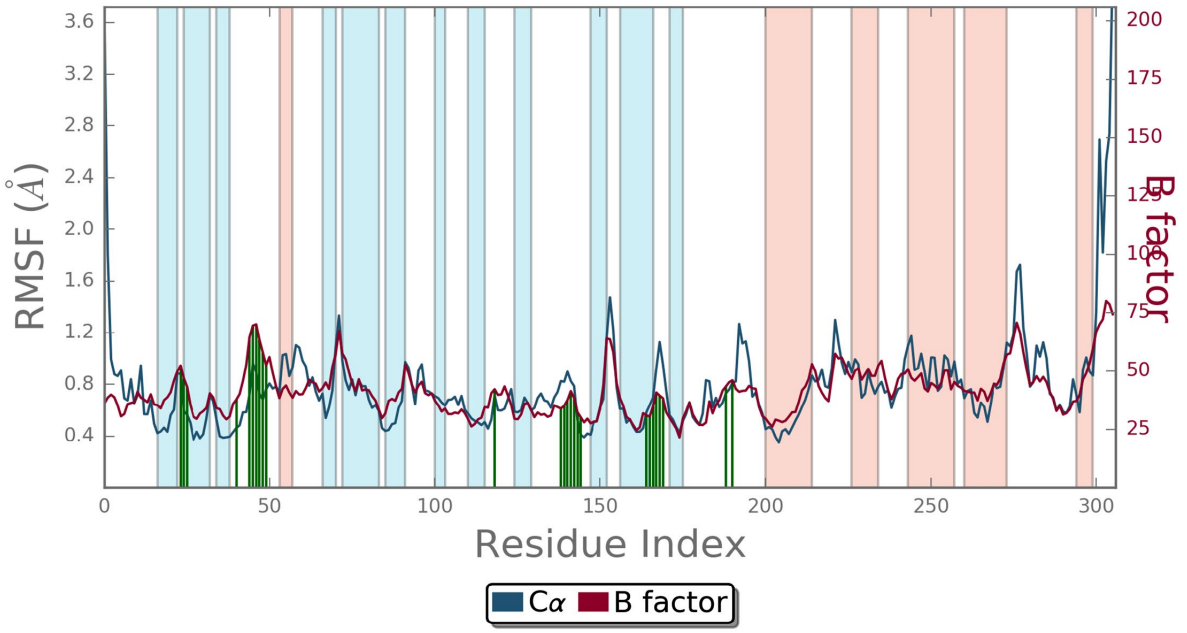

Fig. 7. Root Mean Square Fluctuations (RMSF) of SARS-CoV-2 main protease and its correlation with experimentally determined X-ray B-factor. The point of contact of teicoplanin with protein residues is shown by vertical green lines on X-axis. Loop regions are shown by white bar whereas alpha-helices and beta-sheets are represented in the form of blue and pink bars, respectively.

Structural compactness of the SARS-CoV-2 main protease during MD simulation course was established by evaluation of the radius of gyration (rGyr). Time-dependency plot of the radius of gyration for the simulated system comprising docked teicoplanin in complex with SARS-CoV-2 main protein is shown in Figure 8. It is evident from the plot that there is no significant deviation in the values of rGyr and the compactness of protein is preserved during

the simulated period. Moreover, study of numerous surface areas like molecular surface area (MolSA), polar surface area (PSA), and solvent accessible surface area (SASA) of the complex under study as a function of simulation time also indicate the stability of the teicoplanin-SARS-CoV-2 main protease complex (Figure 8).

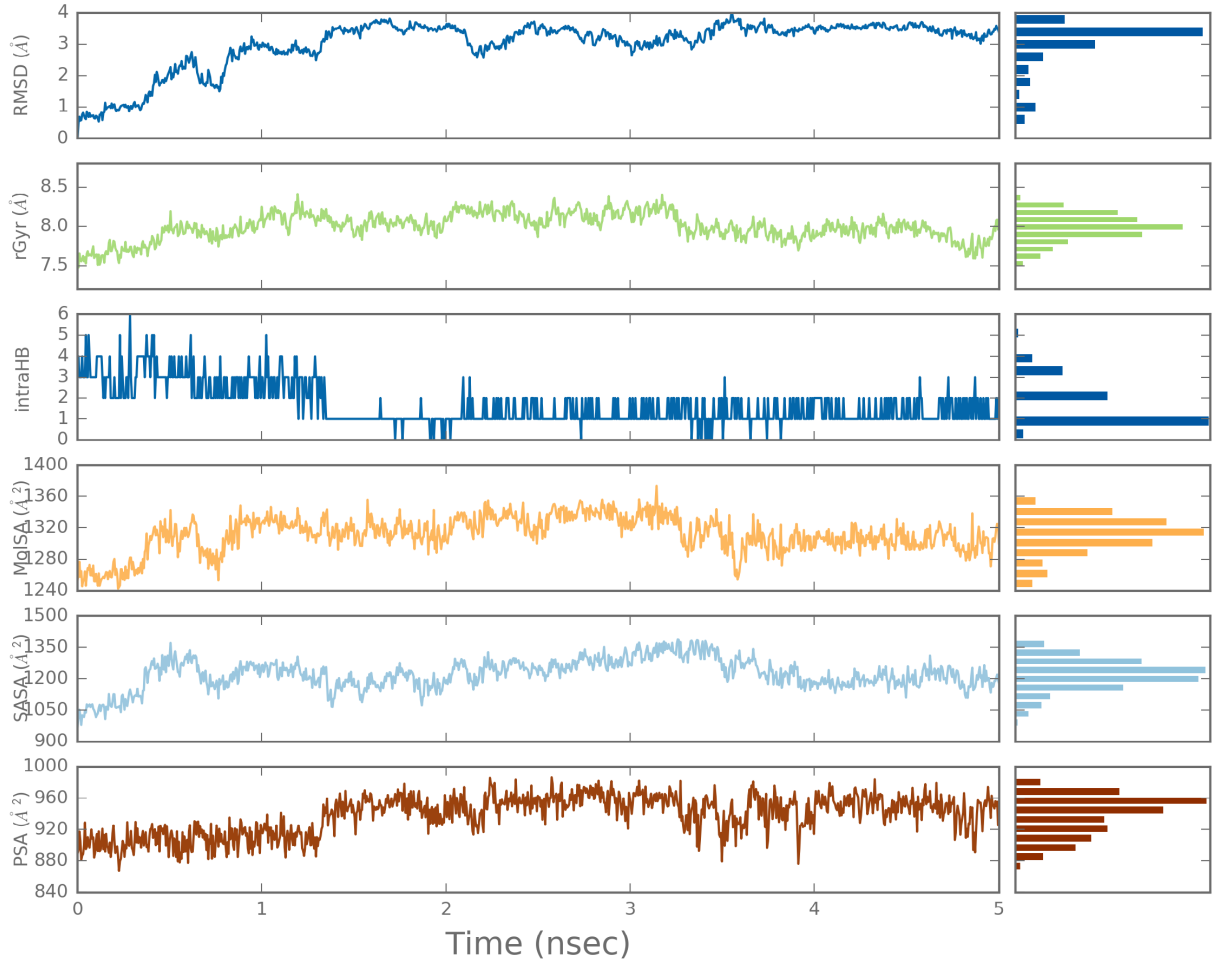

Fig. 8. Root mean square deviation (RMSD) of teicoplanin with respect to the reference conformation; rGyr: Radius of Gyration which measures the 'extendedness' of a ligand; intraHB: Intramolecular Hydrogen Bonds; MolSA: Molecular Surface Area; SASA: Solvent Accessible Surface Area; PSA: Polar Surface Area

Simulation interactions diagrams presented in Figure 9-11 during entire simulation time signifies a comprehensive intermolecular interaction profile of teicoplanin within the

inhibitor binding cavity of SARS-CoV-2 main protease. The modus of interaction pattern of teicoplanin clearly illustrates that the docking predicted main contacts are nearly preserved throughout the MD simulation time of 5ns (Figure 9-11).

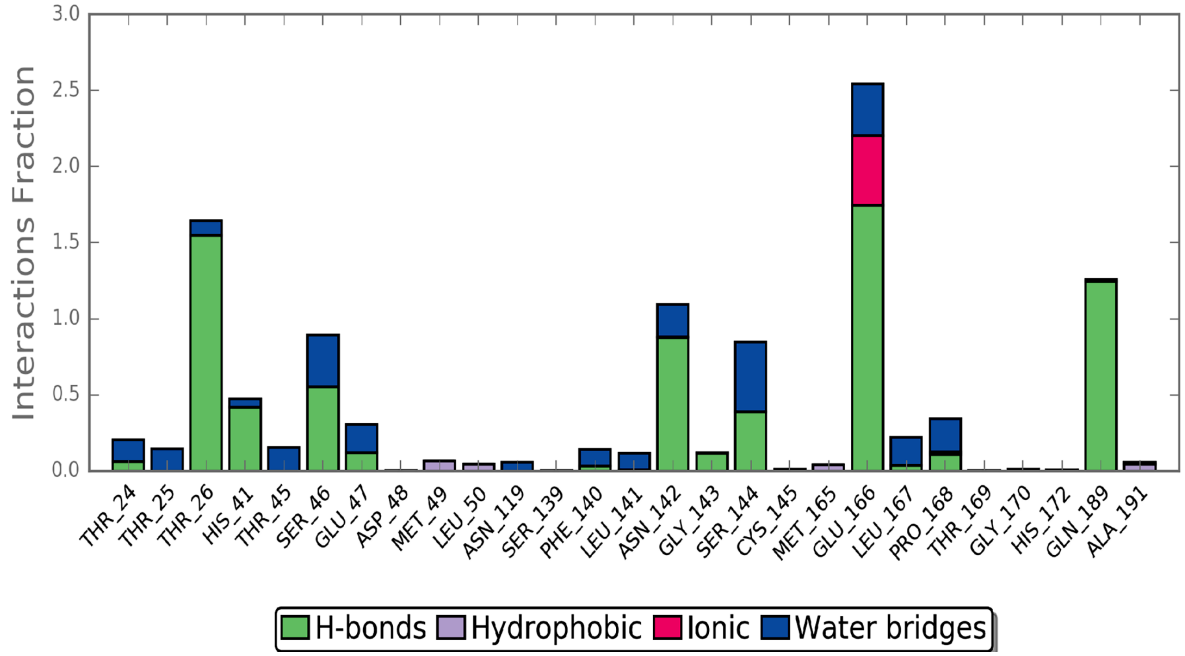

Fig. 9. Protein interactions with teicoplanin, monitored throughout the simulation trajectory. These interactions are clustered by type and summarized in bar diagram including H-bonds, hydrophobic, ionic and water bridges.

Amino acid residues such as Thr26, His41, Ser46, Asn142, Ser144, Glu166 and Gln189 were contributors of the hydrogen bond interaction which is regarded as vital for stability of the bound ligand inside the inhibitor binding pocket of the protein. Several water bridges were also afforded by Thr24, Thr26, His41, Thr45, Ser46, Glu47, Asn119, Phe140, Leu141, Asn142, Ser144, Glu166, Leu167 and Pro168 residues. In addition, hydrophobic contacts were maintained by Met49, Leu50, Cys145, Met165 and Ala191.

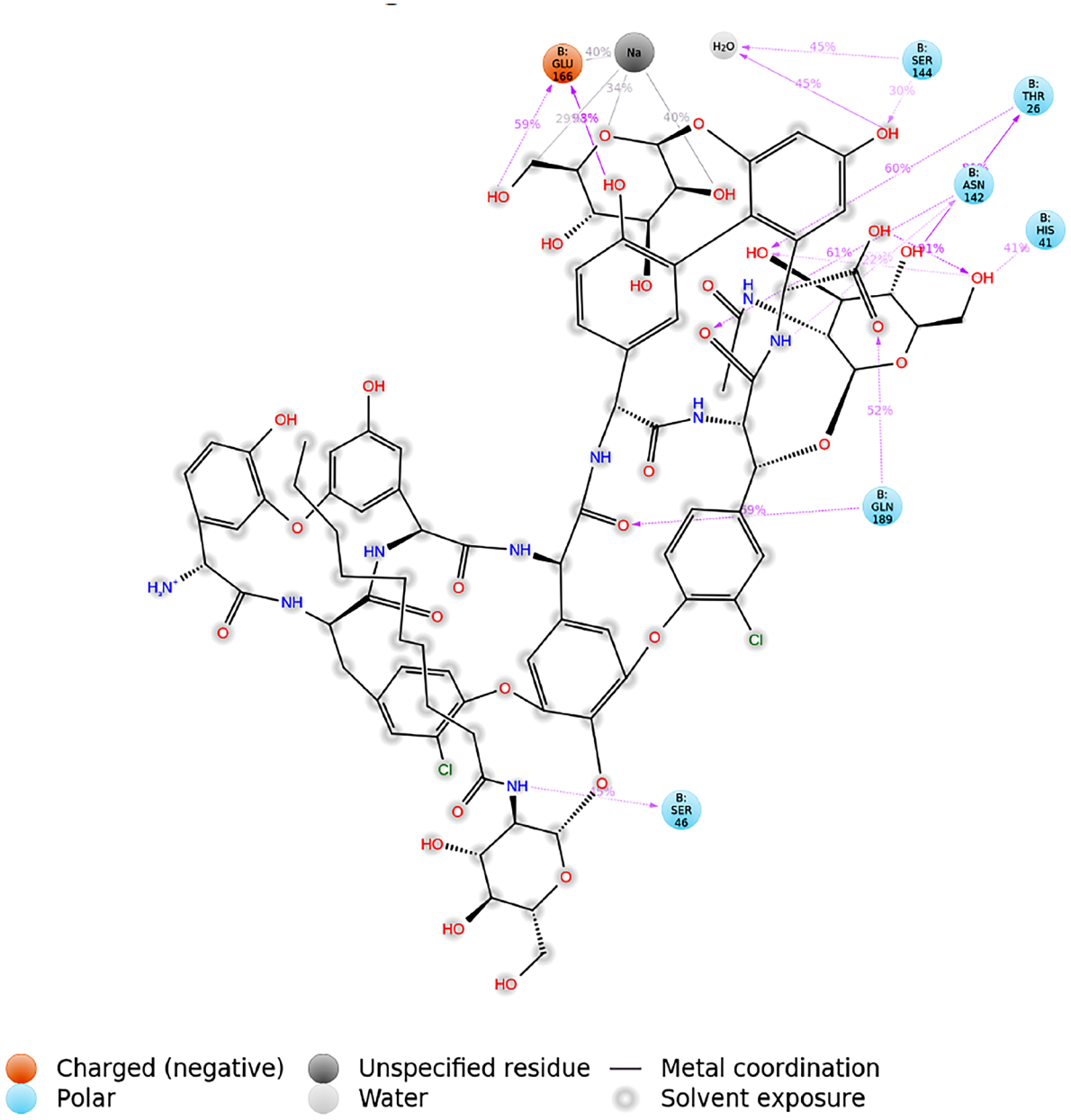

Fig. 10. Two-dimensional representation of atomic interactions between teicoplanin and SARS-CoV-2 protein residues during 5 ns molecular dynamics simulation.

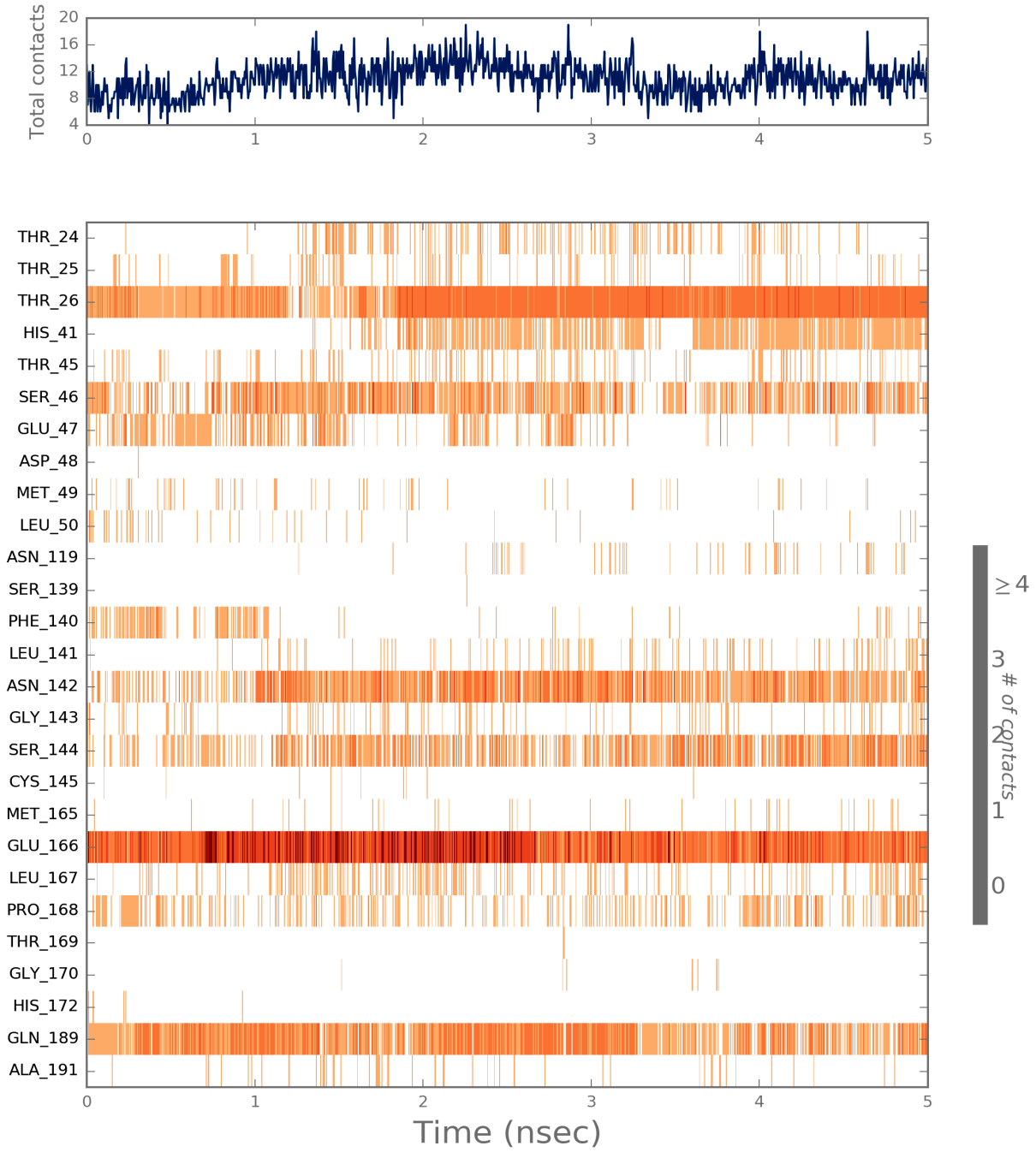

Fig. 11. A timeline representation of the interactions and contacts (H-bonds, Hydrophobic, Ionic, Water bridges) it shows the residues of SARS-CoV-2 main protease interacting with the teicoplanin in each trajectory frame. Some residues make more than one specific contact with the ligand, which is represented by a darker shade of orange, according to the scale to the right of the plot.

Conclusion

By using computer-aided drug design techniques, current study explains the intermolecular interaction of antibacterial drug, teicoplanin with SARS-CoV-2 main protease. Molecular docking studies employing three diverse software namely AutoDock 4.2, AutoDock Vina and Dock 6.9 highlights the importance of hydrophilic and hydrophobic interactions in supporting the teicoplanin molecule inside the inhibitor binding cavity of the SARS-CoV-2 main protease. Molecular dynamics simulation results afforded by Desmond program not only reinforce the credibility of the docking results, but also authenticate the stability of the simulated system, supporting the potential *in vitro* inhibitory activity of teicoplanin against SARS-CoV-2.

Acknowledgements

Nil.

Disclosure statement

No potential conflict of interest was reported by the authors.

References

Aanouz, I.; Belhassan, A.; El Khatabi, K.; Lakhlifi, T.; El Idrissi M.; & Bouachrine, M. (2020) Moroccan Medicinal plants as inhibitors of COVID-19: Computational investigations, *Journal of Biomolecular Structure and Dynamics*, DOI: 10.1080/07391102.2020.1758790

Ahmed MA, Azam F, Rghigh AM, Gbaj A, & Zetrini AE. (2012) Structure-based design, synthesis, molecular docking, and biological activities of 2-(3-benzoylphenyl) propanoic acid derivatives as dual mechanism drugs. *Journal of Pharmacy and Bioallied Sciences*. *4(1)*, 43–50. DOI:10.4103/0975-7406.92728

Ahmed, M., Azam, F., Gbaj, A., Zetrini, A. E., Abodlal, A. S., Rghigh, A., Elmahdi, E., Hamza, A., Salama, M., & Bensaber, S. M. (2016). Ester Prodrugs of Ketoprofen: Synthesis, In Vitro Stability, In Vivo Biological Evaluation and In Silico Comparative Docking Studies Against COX-1 and COX-2. *Current Drug Discovery Technologies. 13*, 41–57. DOI: 10.2174/1570163813666160119092807

Allen, W.J.; Fochtman, B.C.; Balius, T.E.; & Rizzo, R.C. Customizable de novo design strategies for DOCK: Application to HIVgp41 and other therapeutic targets. (2017) *Journal of Computational Chemistry. 38*, 2641-2663. DOI: 10.1002/jcc.25052.

Azam F, Abodabos HS, Taban IM, Rfieda AR, Mahmood D, Anwar MJ, Khan S, Sizochenko N, Poli G, Tuccinardi T, & Ali HI (2019) Rutin as promising drug for the treatment of Parkinson's disease: an assessment of MAO-B inhibitory potential by docking, molecular dynamics and DFT studies, Molecular Simulation, 45:18, 1563-1571, DOI: 10.1080/08927022.2019.1662003

Azam F, Alabdullah NH, Ehmedat HM, Abulifa AR, Taban I, & Upadhyayula S. (2018) NSAIDs as potential treatment option for preventing amyloid β toxicity in Alzheimer's disease: an investigation by docking, molecular dynamics, and DFT studies, *Journal of*

Biomolecular Structure and Dynamics, *36:8*, 2099-2117, DOI: 10.1080/07391102.2017.1338164

Azam, F., Mohamed, N., & Alhussen, F. (2015). Molecular interaction studies of green tea catechins as multitarget drug candidates for the treatment of Parkinson's disease: computational and structural insights. *Network. 26*, 97–115. DOI: 10.3109/0954898X.2016.1146416

Azam, F., Prasad, M.V.V., & Thangavel, N. (2012). Structure-based design, synthesis and molecular modeling studies of 1-(substituted aryl)-3-(thiazol-2-yl)urea derivatives as novel anti-Parkinsonian agents. *Medicinal Chemistry. 8*, 1057–68. DOI: 10.2174/1573406411208061057

Bowers, K. J., Chow, E., Xu, H., Dror, R. O., Eastwood, M. P., Gregersen, B. A., Klepeis, J. L., Kolossvary, I., Moraes, M. A., Sacerdoti, F. D., Salmon, J. K., Shan, Y., & Shaw, D. E. (2006). Scalable algorithms for molecular dynamics simulations on commodity clusters. *Proceedings of the ACM/IEEE Conference on Supercomputing (SC06), Tampa, Florida*, November 11–17. DOI: 10.1145/1188455.1188544

Desmond Molecular Dynamics System, version 2018.4, D. E. Shaw Research, New York, NY.

Elfiky A.A. (2020) SARS-CoV-2 RNA dependent RNA polymerase (RdRp) targeting: An in silico perspective, *Journal of Biomolecular Structure and Dynamics*, DOI: 10.1080/07391102.2020.1761882

Enmozhi, S.K.; Raja, K.; Sebastine, I. & Joseph, J. (2020) Andrographolide As a Potential Inhibitor of SARS-CoV-2 Main Protease: An In Silico Approach, *Journal of Biomolecular Structure and Dynamics*, DOI: 10.1080/07391102.2020.1760136

Fahmy, N.M., Al-Sayed, E., Moghannem, S., Azam, F., El-Shazly, M., Singab, A.N. (2020) Breaking Down the Barriers to a Natural Antiviral Agent: Antiviral Activity and Molecular Docking of Erythrina speciosa Extract, Fractions, and the Major Compound. *Chemistry and Biodiversity*. *17(2)*, e1900511. DOI:10.1002/cbdv.201900511

Harder, E., Damm, W., Maple, J., Wu, C., Reboul, M., Xiang, J.Y., Wang, L., Lupyan, D., Dahlgren, M. K., Knight, J. L., Kaus, J. W., Cerutti, D. S., Krilov, G., Jorgensen, W. L., Abel, R., & Friesner, R. A. (2016). OPLS3: a force field providing broad coverage of druglike small molecules and proteins. *Journal of Chemical Theory and Computation, 12*, 281–296. DOI: 10.1021/acs.jctc.5b00864

Hoover, W.G. (1985) Canonical dynamics: equilibrium phase-space distributions, *Physics Review A. 31*, 1695–1697. DOI: 10.1103/PhysRevA.31.1695

Hospital, A., Goñi, J.R., Orozco, M., & Gelpí, J.L. (2015). Molecular dynamics simulations: advances and applications. *Advances and Applications in Bioinformatics and Chemistry*. *8*, 37–47. DOI: 10.2147/AABC.S70333.

Huang C, Wang Y, Li X, Ren L, Zhao J, Hu Y. et al. Clinical features of patients infected with 2019 novel coronavirus in Wuhan, China. Lancet 2020;395(10223):497–506. doi:10.1016/S0140-6736(20)30183-5.

Humphreys, D.D., Friesner, R.A., & Berne, B.J. (1994). A multiple-time-step molecular dynamics algorithm for macromolecules. *Journal of Physical Chemistry*. *98*, 6885–6892. DOI: 10.1021/j100078a035.

Hussain, M. S, Azam, F., Ahamed, K. F., Ravichandiran, V., & Alkskas, I. (2016). Anti-endotoxin effects of terpenoids fraction from Hygrophila auriculata in lipopolysaccharide-induced septic shock in rats. *Pharmaceutical Biology. 54*, 628–36. DOI: 10.3109/13880209.2015.1070877

Jin, Z., Du, X., Xu, Y., Deng, Y., Liu, M., Zhao, Y., Zhang, B., Li, X., Zhang, L., Peng, C., Duan, Y., Yu, J., Wang, L., Yang, K., Liu, F., Jiang, R., Yang, X., You, T., Liu, X., Yang, X., Bai, F., Liu, H., Liu, X., Guddat, L., Xu, W., Xiao, G., & Qin, C. (2020) Structure of Mpro from COVID-19 virus and discovery of its inhibitors. *Biorxiv*. DOI: 10.1101/2020.02.26.964882

Lu IL, Mahindroo N, Liang PH, Peng YH, Kuo CJ, Tsai KC. et al. Structure-based drug design and structural biology study of novel nonpeptide inhibitors of severe acute respiratory syndrome coronavirus main protease. J Med Chem 2006;49(17):5154–5161. doi:10.1021/jm060207o

Martyna, G.J., Tobias, D.J., & Klein, M.L. (1994) Constant pressure molecular dynamics algorithms. *Journal of Chemical Physics, 101*, 4177-4189. DOI: 10.1063/1.467468

Morris, G. M., Goodsell, D. S., Halliday, R. S., Huey, R., Hart, W. E., Below, R. K., & Olson, A. J. (1998). Automated docking using a Lamarckian genetic algorithm and an

empirical binding free energy function. *Journal of Computational Chemistry. 19*, 1639–62. DOI: 10.1002/(SICI)1096-987X(19981115)19:14<1639::AID-JCC10>3.0.CO;2-B

O'Boyle, N. M., Banck, M., James, C. A., Morley, C., Vandermeersch, T., & Hutchison, G. R. (2011). Open Babel: An open chemical toolbox. *Journal of Cheminformatics*, *3*, 33. DOI: 10.1186/1758-2946-3-33

Raoult D, Hsueh PR, Stefani S, Rolain JM. COVID-19 Therapeutic and Prevention. Int J Antimicrob Agents 2020;105937. doi:10.1016/j.ijantimicag.2020.105937

Shushni, M. A., Azam, F., & Lindequist, U. (2013). Oxasetin from Lophiostoma sp. of the Baltic Sea: identification, in silico binding mode prediction and antibacterial evaluation against fish pathogenic bacteria. *Natural Product Communications. 8*, 1223–6. DOI: 10.1177/1934578X1300800909

Wahedi, H.M., Ahmad, S. & Abbasi, S.W. (2020) Stilbene-based Natural Compounds as Promising Drug Candidates against COVID-19, *Journal of Biomolecular Structure and Dynamics*, DOI: 10.1080/07391102.2020.1762743

Yang H, Xie W, Xue X, Yang K, Ma J, Liang W. et al. Design of wide-spectrum inhibitors targeting coronavirus main proteases. PLoS Biol 2005;3(10):e324. doi:10.1371/journal.pbio.0030324

Zhang J, Ma X, Yu F, Liu J, Zou F, Pan T, et al. Teicoplanin potently blocks the cell entry of 2019-nCoV. BioRxiv 2020. doi: 10.1101/2020.02.05.935387.

Zhou N, Pan T, Zhang J, Li Q, Zhang X, Bai C. et al. Glycopeptide Antibiotics Potently Inhibit Cathepsin L in the Late Endosome/Lysosome and Block the Entry of Ebola Virus, Middle East Respiratory Syndrome Coronavirus (MERS-CoV), and Severe Acute Respiratory Syndrome Coronavirus (SARS-CoV). J Biol Chem 2016;291(17):9218–9232. doi:10.1074/jbc.M116.716100